ChemComm

Accepted Manuscript

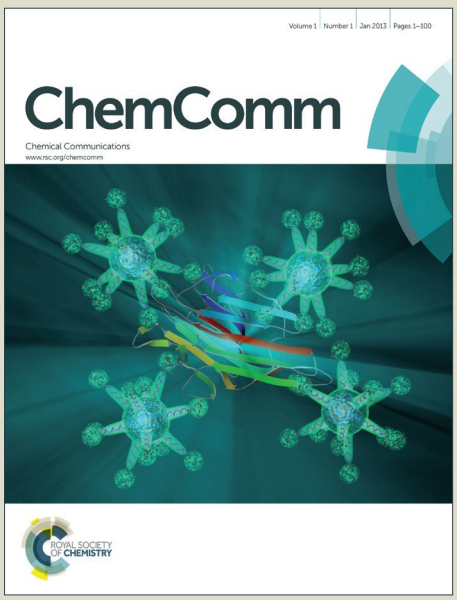

ROYAL SOCIETY OF CHEMISTRY

www.rsc.org/chemcomm

Journal Name

COMMUNICATION

Highly efficient hydrogen production through ethanol photoreforming by a carbon nanocones/Pd@TiO_2 hybrid catalyst

Received 00th January 20xx,
Accepted 00th January 20xx

DOI: 10.1039/x0xx00000x

www.rsc.org/

M. Melchionna,[*a] A. Beltram,[a] T. Montini,[a] M. Monai,[a] L. Nasi,[b] P. Fornasiero,[*a] and M. Prato[*a]

Production of molecular hydrogen (H_2) is becoming an increasingly prominent process, due to the high expectations as a new green energy carrier and key reagent for many industrial processes. Herein we report the high efficiency in the H_2 production via photoreforming of ethanol by a catalyst based on hierarchical carbon nanocones hybridised with an inorganic layer of nanocristallineTiO_2containing Pd nanoparticles.

Carbon nanostructures (CNSs) have emerged in the last 10 years as intriguing building blocks in the assembly of nanohybrids or nanocomposites for a variety of different applications, such as organic photovoltaic systems,[1] integrated circuits, [2] biosensors[3] and nanomedicine.[4] Catalysis has also been enjoying a great momentum, with attention particularly focused on the use of carbon nanotubes (CNTs) and graphene (G), although more recent efforts have brought to light materials based on other structures such as carbon nanohorns, carbon quantum dots and carbon nanofibers.[5]

In this context, carbon nanocones (CNCs) represent a very peculiar class of carbon nanostructures. They have been known since almost two decades,[6] and a few recent theoretical studies modelled their physical properties, predicting a great potential for exploitation in several applicative fields. Indeed, it was highlighted that their cone-like morphology results in very interesting features, such as an uncommon graphene sheet stacking depending on the apex (cone) angle[7] or a potential for hydrogen storage.[8] To the best of our knowledge, there are no reports on the utilization of CNCs as supports for metal catalysts, which might open new perspectives. Their unique shape and the absence of bundling processes such as those found in CNTs are expected to result in easier manipulation as well as improved activity in several energy-related catalytic transformations. Furthermore, by controlled alignment of CNCs it is possible to enhance their conductivity by 2-3 order of magnitude [9] with great implication in energy related applications. From the energy point of view, the sustainable production of H_2 represents a very hot topic, given the predicted future role of H_2 as energy carrier able to replace the depleting fossil fuel resources. Moreover, H_2 is an important molecule for the industrial sector, extensively used in the synthesis of ammonia and fertilizers, in the hydrogenation reactions for fine chemicals and in oil refining. The generation of H_2 through the use of light and biomass-derived alcohols (photoreforming) comes across as a promising sustainable possibility.[10] In this work, we report the successful synthesis of a hierarchical nanostructured catalyst based on the hybridization of CNCs with an inorganic phase consisting of Pd nanoparticles immersed into nanocristalline TiO_2 and we show their outstanding activity towards photoreforming of ethanol. Despite the use of Pd in lieu of the more expensive and traditional Pt, the performance is amongst the highest ever reported for CNSs-based catalysts, largely surpassing (almost 5 times higher) that of analogous systems reported under the similar experimental conditions by our group consisting of CNTs/Pt@TiO_2 even using the more challenging ethanol as sacrificial agent and the traditionally less active Pd (instead of Pt).[11] The high activity is the result of a well-engineered interplay between the three phases, which are in intimate contact with each other. An effective electron sink effect, provided by the CNCs that retards the photoexcited charge carriers recombination, combines with the highly active core-shell structure of the Pd@TiO_2 component, resulting in exceptional performances. However, given the lower conductivity of CNCs compared to CNTs or G, the high performance must arise from other distinct factors. It is expected that the improved dispersibility in liquid media (which also determines a more controlled synthetic protocol and a better reproducibility) results in a more homogeneous final structure as compared to other nanocarbons, with an enhanced numbers of heterojunctions at the CNC/TiO_2 interface and therefore an improved activity. In addition, we show that the catalysts are active

[a] Department of Chemical and Pharmaceutical Sciences, INSTM, ICCOM-CNR, University of Trieste, Via L. Giorgieri 1, 34127 Trieste, Italy.
[b] CNR-IMEM Institute, Parco area delle Scienze 37/A, 43124 Parma, Italy

† Footnotes relating to the title and/or authors should appear here.
Electronic Supplementary Information (ESI) available: Synthesis, additional characterisation and solar photocatalytic activity Fig S1-S6 and Table S1. See DOI: 10.1039/x0xx00000x

under simulated solar light, which may inspire future developments in solar cell assembly.

CNCs morphology varies according to the cone angle, which in turns implies presence of a certain number of pentagons within the 6-membered ring patterns to create the conical geometry. The angle can reach 0°, in absence of pentagons with a resulting disk-like geometry. CNCs are normally obtained as a mixture of the various structures possessing the different geometrical parameters, with a large excess (about 70%) of disk-like structures. The mixture produced by the n-TEC company and containing both disks and cones was used in the present work. The CNCs used here were previously oxidised to produce COOH groups, in order to secure the firm anchoring of the inorganic phase (**ox-CNCs**).

The final hybrids were prepared via a sol-gel method, where the preformed Pd@TiO_2 precursors were added while sonicating to a dispersion of ox-CNCs in ethanol. Final controlled hydrolysis and purification afforded **ox-CNCs/Pd@TiO_2**. Crystallization of the TiO_2 shell and removal of the organic groups was performed through calcination at 350°C for 5 hours (**ox-CNCs/Pd@TiO_2-350**). The nominal Pd content was fixed to 1%wt (see SI).

Thermogravimetric analysis (TGA) revealed a very close match to the theoretical mass composition, with the CNCs accounting for 21% wt in **ox-CNCs/Pd@TiO_2-350**, as observed by the weight loss beginning at ~500 °C due to combustion of the carbon scaffold. As a comparison, the fresh sample **ox-CNCs/Pd@TiO_2** exhibited two well defined weight losses, the first one at ~200 °C, attributable to loss of CO_2 from the carboxylic groups and residual organic moieties from hydrolysis of Ti precursor (Fig S1). Notably, the combustion of **ox-CNCs** starts at higher temperature (600°C), which indicates that the Pd@TiO_2 is capable of catalyse combustion and indirectly proves the tight CNC-TiO_2 contact.

TEM micrographs show that both conical and disk-like structures are well covered, with the oxide layer imparting an increased roughness to the surface (Fig 1). Given their small size and the surrounding thick metal oxide layer, the Pd nanoparticles are not visible by TEM analysis.

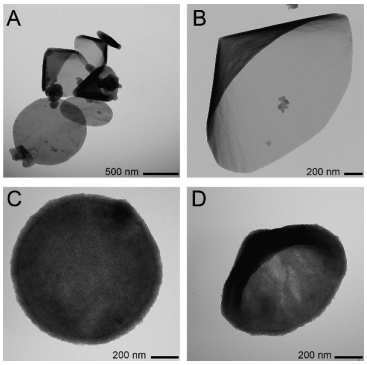

Fig 1. Representative TEM images of **ox-CNCs** with cones and disk-like morphology (A and B) and **ox-CNCs/Pd@TiO_2** in both disk-like (C) and conical (D) morphologies

The presence of Pd is confirmed by EDX mapping, where each individual element (C, Ti, O and Pd) was clearly detected (Fig. 2). Moreover, HRTEM and Fast Fourier Transform (FFT) provide additional confirmation (Fig S2 and S3). The Pd distribution appears to be very diffused all around the structure, confirming the homogeneity of the hybrids and the tight contact between the three phases. HR-TEM combined with SAED evidenced that TiO_2 in **CNCs/Pd@TiO_2-350** is in its anatase phase (Fig. 2D). Analysis of the TiO_2 particles revealed an approximate size range of 6-9 nm.

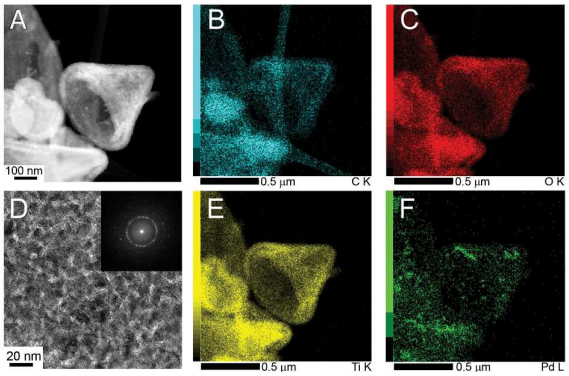

Fig 2. Representative STEM of **ox-CNCs/Pd@TiO_2-350** (A) and HR-TEM area expansion showing anatase phase (D) as confirmed by corresponding Fast Fourier Transform (inset). Representative EDX mapping showing carbon (B), oxygen (C), titanium (E) and palladium (F)

XRD patterns of the calcined sample shows the characteristic reflections of the anatase phase of TiO_2 (Fig S4) with a calculated average crystallite size of 11 nm (applying the Scherrer equation), in good agreement with HR-TEM and Raman analysis (see below). The signature reflection of the graphitic framework of CNC (26.6°) is not distinguishable as it overlaps with the (101) reflection of anatase. A very small reflection around 34° was observed, indicating the presence of another phase at trace level. The position of this reflection suggests that this impurity could be doped/highly defective $FeTi_2O_4$, consistently with the reaction of Ti alkoxide with low level Fe impurities of the CNCs during sol-gel synthesis and calcination. No reflections related to Pd-based phases are observed, presumably because of the low loading.

Raman analysis of ox-CNCs shows the typical fingerprint of the graphenic framework, with the G band and the defect-induced D band at ~1350 cm^{-1}, a consequence of the COOH functionalization (Fig. S5). The I_D/I_G ratio for the CNCs is 0.97. A broad 2D band is visible as a double-peak, suggesting a stacking process of the cones or disks, as also reported for graphene.[12] After functionalization with the Pd@TiO_2 phase, the I_D/I_G ratio slightly decreases (0.93). This effect of "healing" by a metal oxide layer has been previously explained for carbon nanotubes covered with TiO_2, where the decrease of the I_D/I_G was related to a perturbation by oxide layer of the outer CNTs shell, which is therefore not contributing to the intensity of the D band, and which further confirms the excellent interfacing of the two phases.[13] Apart from the I_D/I_G change, no further differences between the CNCs and the **CNCs/Pd@TiO_2** is

observed, indicating that the attached TiO_2 is amorphous. However, the sample after calcination (**CNCs/Pd@TiO_2-350**) shows appearance of new peaks, which are the six vibration modes characteristic for TiO_2 anatase (Fig S6).[14]

Further characterization was carried out by FT-IR (Fig S7). By analogy with CNTs, the CNCs presence even after calcination is supported by the characteristic polyaromatic carbon C=C stretching at ~1598 cm^{-1},[15] while the O-H bending at 3432 cm^{-1} and the C=O stretching at 1727 cm^{-1} confirm the presence of the COOH groups in the **CNCs/Pd@TiO_2** catalyst, while the latter peak almost disappears in the calcined sample.[16] It is interesting to note that upon hybridization with the titanium dioxide, the band relative to the O-H bending increases even in the calcined sample where the COOH groups have been removed, implying that the material can readily adsorb water molecules.[17] The integration of the TiO_2 phase into the nanohybrid is confirmed in both **CNCs/Pd@TiO_2** and **CNCs/Pd@TiO_2-350**, with the peak assigned to the Ti-O-Ti vibration mode (between 600 and 900 cm^{-1}) clearly arising after reaction with the Pd@TiO_2 component. Moreover, after hybridization with the oxide layer, the appearance of a signal at ~1000 cm^{-1} in the profile of **CNCs/Pd@TiO_2** is noted, previously assigned to a Ti-O-C vibrational mode in CNTs-TiO_2 hybrids, which indicate intimate bonding between the carbon support and the TiO_2.[18]

UV-vis spectroscopy also reveals a change of features of the TiO_2 after integration of the CNCs component, with a beneficial shift of the main absorbance peak from 301 nm to 324 nm (Fig S8).

Significant differences have been observed in the N_2 physisorption isotherms (Fig S9), resulting in different textural properties of the materials (Table S1). The pristine oxidized CNCs show Type II isotherm, typical of non-porous/macroporous materials.[19] A relatively low surface area is calculated following the BET model while BJH analysis shows the presence of macropores around 100 nm (Fig S10).

After introducing the Pd@TiO_2 units, the textural properties of the materials completely change. **Ox-CNCs/Pd@TiO_2** shows a Type I isotherm, typical of microporous materials, with a pore size distribution extending to the lower part of the mesoporous range (Fig S9). According to this, a strong increase in the specific surface area is observed, although the increase of pore volume is modest. The increase in the gas adsorption at high p/p_0 values indicates the presence of a certain contribution of macropores. The microporous network in this sample can be clearly related to the Pd@TiO_2 gel covering the CNCs with a not well crystallized structure.

After calcination at 350°C and the crystallization of the TiO_2 phase into anatase, the formation of an extended mesoporous network is observed in the **ox-CNCs/Pd@TiO_2-350** material. The specific surface area of this sample is much lower than that before calcination but, most importantly, pore size and volume are significantly increased. This fact is crucial for the photocatalytic activity, since the formation of mesopores avoids significant diffusional limitations during solid/liquid/gas phases reactions.

The catalytic performance of the two materials **CNCs/Pd@TiO_2** and **CNCs/Pd@TiO_2-350** was investigated in the H_2 evolution from 1:1 v/v solutions of ethanol/water under UV-vis irradiation. Their activity was compared to that of a reference catalyst prepared by applying the same procedure but in the absence of CNCs and calcined at 350°C (**Pd@TiO_2-350**) (Fig 3). Moreover, the performance was compared versus most recent nanocarbon-supported catalysts (Table S2). highlighting the notable improvements reached with the current catalytic system. We reported the production of H_2 over time normalized over the surface area of the specific sample. As demonstrated for a catalyst based on Au/TiO_2, if a merely geometrical effect is responsible for the catalytic activity, normalisation over surface area should result in equivalent activity.[20] In our case, the remarkable difference in activity for the tested catalysts implies that the presence of the CNCs into the Pd@TiO_2 active phase introduces a considerable change in the electronic properties and the improved H_2 production does not depend on simple geometrical changes.

More in details, the highest activity, with an outstanding H_2 production of 5 $mmol \cdot m_{cat}^{-2}$ after 20h (corresponding to 600 $mmol \cdot g_{cat}^{-1}$) was obtained with **CNCs/Pd@TiO_2-350** with a calculated quantum efficiency (QE) of 12.3%. On the other hand, the fresh catalyst (**CNCs/Pd@TiO_2**) displayed much lower activity (~0.5 $mmol \cdot m_{cat}^{-2}$). The reason for this difference stems from the crystallinity of TiO_2 in **CNCs/Pd@TiO_2-350**, where the anatase phase imparts an enhanced photoresponse to UV. It is worth noticing that even if calcined, and therefore with the TiO_2 in anatase phase, the CNC-free catalyst shows an activity comparable to that of the non-calcined sample (**CNCs/Pd@TiO_2**). Thus, the impact of the CNC in the catalytic activity is very evident, together with the importance to perform a calcination treatment, and is ascribed to the extremely proficient electron sink effect which retards charge carrier recombination. Moreover, the stability **CNCs/Pd@TiO_2-350** catalyst is also very pronounced, with evolution rates fully retained over the initial 10 hours of irradiation, before undergoing slight deactivation, presumably due to partial aggregation. As a further term of comparison, the CNTs/Pd@TiO_2 analogues reported by our group for the photoreforming of the usually more active methanol are largely outperformed by **CNCs/Pd@TiO_2-350**, with H_2 production barely overcoming 0.5 $mmol \cdot m_{cat}^{-2}$ after 15 hours of irradiation. This highlights the high proficiency of the CNCs nanostructure, with improved activity attributed to the more efficient and uniform contact between the organic and inorganic phases, as a result of the better dispersibility of CNCs as compared to CNTs, which also causes an improved reproducibility of the catalyst assembly. The recyclability of **CNCs/Pd@TiO_2-350** was evaluated by carrying out three catalytic cycles with the used catalyst (Fig S12). A small deactivation is observed after the first cycle when calculating the rate of H_2 evolution per gram of catalyst, while the second and third cycles display identical performance, indicating a partial

modification of the catalyst after UV irradiation. The deactivation is associated with a decrease (~20%) of the surface area of the catalyst after the first catalytic cycle. When normalised by the surface area, however, the catalytic activity is stable through all the three cycles.

Together with H_2, formation of acetaldehyde and 1,1-diethoxyethane as by-products in both the gas and liquid phases is observed. CH_4 and CO_2 are observed only in traces, indicating that the full dehydrogenation sequence ethanol→acetaldehyde→acetic acid→CO_2 is strongly disfavoured due the poor adsorption of acetaldehyde onto the TiO_2 phase, as previously demonstrated.[21]

When the Pd-free catalyst (**ox-CNC/TiO_2-350**) was employed, only negligible amounts of H_2 were found, confirming the essential role of Pd as truly catalytic site for the proton reduction to H_2.

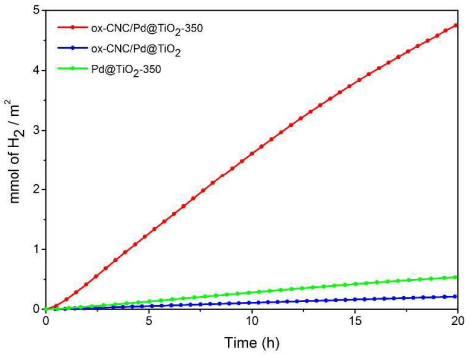

Fig 3. H_2 production over time by **ox-CNCs/Pd@TiO_2**, **ox-CNCs/Pd@TiO_2-350** and **Pd@TiO_2-350** normalised by the initial surface area of the catalyst under UV-Vis illumination.

Notably, catalysis under solar irradiation using **CNCs/Pd@TiO_2-350** also resulted in appreciable H_2 evolution, with production as high as 0.25 mmol·m_{cat}^{-2} (corresponding to 32 mmol·g_{cat}^{-1}) and a long stability over time (Fig S11). The much lower productivity as compared to the UV experiments is easily explained in terms of the smaller UV content (4%) of the sun light, which is the actually absorbed radiation wavelength window. The non-calcined catalyst exhibited a non-detectable activity under these conditions.

In summary, we report the very first example of a hierarchical CNCs based photocatalyst containing Pd@TiO_2 . Very high activity was obtained with the calcined catalyst under UV irradiation, amongst the highest ever reported with carbon-based supports. Other than providing an increased surface area, the enhanced activity is due to the capability of the carbon framework to scavenge away the photoexcited electrons, thus retarding charge recombination rates. However, given the lower conductivity of CNCs relative to CNTs or G, the pronounced activity must be put in relation to other characteristics, above all the easier formation of dispersions in liquid media. This results in a considerable improvement of the homogeneity of the final catalyst structures, with maximised areas of contact of the organic and inorganic phases, and in turn an increased number of heterojunctions, responsible for the higher activity. It is also worth noting that high performances were achieved using an environmental friendly sacrificial donor such as ethanol, a product of fermentation from feedstock (corn, sugarcane etc.). The catalysts also show good activity under solar irradiation, propelling them as promising starting points for solar fuel cells development.

The research leading to these results has received funding from the Seventh Framework Programme [FP7/2007- 2013] under grant agreement n° 310651 (SACS project). We thank the Norwegian company n-TEC for providing the CNCs samples.

Notes and references

1 (a) L. M. Dai, D. W. Chang, J. B. Baek, W. Lu, *Small*, 2000, **8**, 1130; (b) S. Cataldo, P. Salice, E. Menna, B. Pignataro, *Energy Environ. Sci.*, 2012, **5**, 5919.
2 (a) Z. Liu, L. Jiao, Y. Yao, X. Xian, J. Zhang, *Adv. Mater.,* 2010, **22**, 2285; (b) P. Avouris, *Phys. Today*, 2009, **62**, 34; (c) A. M. Rawlett, T. J. Hopson, I. Amlani, R. Zhang, J. Tresek, L. A. Nagahara, R. K. Tsui, H. Goronkin, *Nanotechnology*, 2003, **14**, 377.
3 Z. Chen, X. Zhang, R. Yang, Z. Zhu, Y. Chen, W. Tan, *Nanoscale*, 2011, **3**, 1949.
4 (a) C. Fabbro, H. Ali-Boucetta, T. Ros, K. Kostarelos, A. Bianco, M. Prato, *Chem. Commun*., 2012, **48**, 3911; (b) A. Montellano, T. Da Ros, A. Bianco, M. Prato, *Nanoscale*, 2011, **3**, 4035.
5 M. Melchionna, M. Bonchio, F. Paolucci, M. Prato, P. Fornasiero, *Top. Curr. Chem.,* 2014, **348**,139.
6 A. Krishnan , E. Dujardin , M. M. J. Treacy , J. Hugdahl , S. Lynum ,T. W. Ebbesen, *Nature* 1997, **388**, 451.
7 (a) C.-T. Lin, C.-Y. Lee, H.-T. Chiu, T.-S. Chin, *Langmuir,* 2007, **23**, 12806;
8 A. S. Shalabi, K. A. Soliman and H. O. Taha *Phys. Chem. Chem. Phys*., 2014, **16**, 19333.
9 ACS Appl. Mater. Interfaces, 2011, 3 (2), pp 378–384
10 M. Cargnello, A. Gasparotto, V. Gombac, T. Montini, D. Barreca, P. Fornasiero, *Eur. J. Inorg. Chem.*, 2011, **28**, 4309.
11 M. Cargnello, M. Grzelczak, B. Rodrıguez-Gonzalez, Z. Syrgiannis, K. Bakhmutsky, V. La Parola, L. M. Liz-Marzan, R. J. Gorte, M. Prato, P. Fornasiero *J. Am. Chem. Soc*., 2012, **134**, 11760.
12 A. C. Ferrari, J. C. Meyer, V. Scardaci, C. Casiraghi, M. Lazzeri, F. Mauri, S. Piscanec, D. Jiang, K. S. Novoselov, S. Roth, A. K. Geim, *Phys. Rev. Lett.*, 2006, **97**, 187401.
13 F. Inoue, R. A. Ando, P. Corio, *J. Raman Spectrosc*, 2011, **42**, 1379.
14 (a) T. Ohsaka, F. Izumi, Y. Fujiki, *J. Raman Spectrosc*., 1978, **7**, 321; (b) O. Frank, M. Zukalova, B. Laskova, J. Kurti, J. Koltai, L. Kavan *Phys. Chem. Chem. Phys*., 2012, **14**, 14567.
15 M. Shaffer, X. Fan, A. Windle, *Carbon*, 1998, **36**, 1603.
16 (a) Y. Li, C. Xu, B. Wei, X. Zhang, M. Zheng, D. Wu, P. M. Ajayan, *Chem. Mater*., 2002, **14**, 483.
17 J. Shen, B. Yan, M. Shi, H. Ma, Na Li, M. Ye, *J. Mater. Chem*., 2011, **21**, 3415.
18 R. Urlaub, U. Posset, and R. Thull, *J. Non-Cryst. Solids*, 2000, **265**, 276.
19 K. S. W. Sing, D. H. Everett, R. A. W. Haul, L. Moscou, R. A. Pierotti, J. Rouquerol, T. Siemieniewska, *Pure Appl. Chem.*, 1985, **57**, 603.
20 M.A. Nadeem, M. Murdoch, G.I.N. Waterhouse, J.B. Metson, M.A. Keane, J. Llorca, H. Idriss *J Photoch Photobio A* 2010, **216**, 250.
21 G.L. Chiarello, M. H. Aguirre, E. Selli, *J. Catal*., 2010, **273**, 182.